

Investigating the leptonic couplings of doubly charged scalars at the muon collider

Nivedita Ghosh^{a,*}, Santosh Kumar Rai^{b,†}, Tousik Samui^{c,‡}, Agnivo Sarkar^{b,§}

^a*Kavli IPMU (WPI), UTIAS, University of Tokyo, Kashiwa, Chiba, 277-8583, Japan*

^b*Regional Centre for Accelerator-based Particle Physics, Harish-Chandra Research Institute,
A CI of Homi Bhabha National Institute, Chhatnag Road, Jhansi, Prayagraj 211019, India*

^c*The Institute of Mathematical Sciences, IV Cross Road, CIT Campus, Taramani, Chennai 600113, India*

Abstract

We study the lepton flavor conserving and violating couplings of a doubly charged scalar at a 3 TeV muon collider. Using a model-independent Lagrangian, we analyze the ee , $\mu\mu$, and $\tau\tau$ final states mediated by the doubly charged scalar to probe individual couplings to μe , $\mu\mu$, and $\mu\tau$. We find that for a doubly charged scalar of mass greater than 1 TeV and $\mathcal{O}(1)$ couplings, we achieve high signal significance in these channels. We delineate the collider's sensitivity in the mass-coupling plane, highlighting the extensive reach of the muon collider in probing these couplings far beyond the current experimental limits. We also propose an angular distribution variable to discriminate the exchange of a doubly charged scalar from that of a neutral scalar, which give identical signals.

1 Introduction

The discovery of the Higgs boson at the Large Hadron Collider (LHC) [1, 2] marked a significant milestone in particle physics, confirming the mechanism by which elementary particles acquire mass within the Standard Model (SM). However, notwithstanding its various experimental confirmations, SM still leaves many unanswered questions, including the mechanism for neutrino masses. To address this, various extensions to the SM have been proposed in the literature, one of which is the Higgs Triplet Model (HTM) [3–5]. This model introduces a triplet scalar field, which includes a doubly charged Higgs boson. The primary motivation for considering the HTM and the doubly charged Higgs lies in its role within the type-II seesaw mechanism [6], which provides a natural explanation for the smallness of neutrino masses through the vacuum expectation value (VEV) of the scalar triplet. Beyond the HTM, the doubly charged Higgs also appears in the Left-Right Symmetric Model (LRSM), which extends the gauge group to $SU(2)_L \times SU(2)_R \times U(1)_{B-L}$, proposing a symmetry between left- and right-handed particles and includes triplet scalars [7–11]. In LRSM, both the $SU(2)_L$ and $SU(2)_R$ scalar triplets can include doubly charged components, with the $SU(2)_R$ triplet's VEV potentially at the TeV scale

*nivedita.ghosh@ipmu.jp

†skrai@hri.res.in

‡tousiks@imsc.res.in

§agnivosarkar@hri.res.in

to provide masses for right-handed gauge bosons. The LRSM model also addresses the strong CP problem and parity violation, further motivating the study of doubly charged Higgs bosons. Other notable models include doubly charged scalars, which can generate neutrino masses through a radiative mechanism [12–18].

The ATLAS [19–23] and CMS [24–28] collaborations have searched for these doubly charged scalars $H^{\pm\pm}$ in both pure leptonic as well as $W^\pm W^\pm$ final states. One can note that in the majority of these searches, pair production of the doubly charged scalars via the Drell-Yan mode remains the primary production mode. A doubly charged scalar can also be produced at the LHC via associated and vector boson fusion modes. However, in comparison to Drell-Yan mode, these production channels depend on how the electroweak symmetry is broken in the underlying model. A comprehensive analysis considering all these channels at the LHC and their sensitivity in the mass vs. coupling plane $\{m_{H^{\pm\pm}}, h_{XY}\}$ plane can be found in Ref. [29]. The experiment has been able to probe the doubly charged scalar up to masses of $\mathcal{O}(\text{TeV})$. The major obstacle that the LHC faces in excluding very large values of $m_{H^{\pm\pm}}$ or much smaller values h_{XY} couplings is due to the center of mass (c.o.m) being not sufficient enough to pair produce these relatively heavier leptophilic exotic scalars with large enough rates. Thus, one has to look for an alternative collider that can surpass these challenges of the pure hadronic machine.

In contrast, if one considers a leptonic collider [30–37], then one can think of an alternative signal channel e.g. $\ell_a^+ \ell_a^- \rightarrow \ell_i^+ \ell_j^-$ (where $a = e, \mu$ and $i, j = e, \mu, \tau$), where the doubly charged scalar participates in a t -channel process. The advantage of this channel is two fold – (i) *in lieu* of pair production, a single $H^{\pm\pm}$ is participating, and (ii) as the signal channel is mediated via t -channel $H^{\pm\pm}$, this machine will be able to probe $m_{H^{\pm\pm}} \geq \sqrt{s}$ (c.o.m of the lepton collider) region. These aspects motivate us to conduct our study in the context of a lepton collider [38–45]. If one considers the first generation lepton collider that is e^+e^- circular collider, then at very high energies, the large synchrotron radiation will restrict the availability for very high energy collisions significantly, limiting the reach for BSM searches. Even at the proposed linear colliders for e^+e^- collisions, beam radiation will be a major issue. A second-generation lepton collider (or in other words, $\mu^+\mu^-$ collider) seems like the next best alternative that could achieve very high-energy collisions with much less synchrotron radiation or beam effects.

The proposal for the high-energy muon collider by the *International Muon Collider Collaboration* (IMCC) [46–51] is a timely proposal going worldwide. The reason behind the popularity of this collider comes from the fact that it can offer the advantages of both the lepton collider as well as the hadron collider [52–59]. To elaborate the advantages, let us first compare it to hadron colliders. The muon collider will ideally be more efficient at high energies because it can use all of the machine’s energy, unlike hadron colliders, where the beam energy is shared amongst the partons that participate in the hard scattering processes with effectively lower energies. Also, at the muon colliders, one expects to have a much more precise kinematic information regarding the initial state colliding particles. In addition, hadron colliders face a lot of unsolicited noise from hadronic activity and the smearing caused by parton distribution functions (PDFs), making precision studies hard. The muon can produce high center-of-mass energies in collisions with very little energy spread due to reduced bremsstrahlung and beamstrahlung effects [60, 61], as the mass of the muon is appreciably higher than that of the electron. Although the energy and luminosity of the muon collider are not finalized yet, there is proposal to run it with 1 ab^{-1} luminosity at 3 TeV c.o.m energy and 10 ab^{-1} luminosity for a 10 TeV machine [52, 53, 62]. With this first-ever proposal of a second-generation lepton collider, one hopes to discover new physics (NP) scenarios that HL-LHC might not be able to probe [63–78].

In this paper, our goal is to investigate the possible physics prospect that the future muon collider offers, specifically targeting the scalar sector of different BSM models, which can embed a leptophilic

charged scalar. To do so, we will consider a class of BSM scenarios where the SM particle spectrum is enlarged with at least one pair of doubly charged scalar particles. In the context of LHC, there are already many recent works that search for the doubly charged scalars [79–83]. However, dedicated analysis to probe the doubly charged scalar and its couplings at a muon collider are very few in the literature [84–86].

In this work, we attempt to find answers to the following questions:

1. Can a future muon collider with 1 ab^{-1} luminosity at **3 TeV c.o.m** energy show significant improvement in terms of probing the leptonic coupling of the doubly charged scalar?
2. Since we focus on an off-shell exchange of the doubly charged scalar, there could potentially be other (NP) particles that contribute to similar final states that we choose for our analysis. What are the possible ways to disentangle the NP source in the context of the current study at the muon collider?

The article is organized in the following fashion - in section 2 we introduce the theoretical set up for our study and determine the allowed region in the $\{m_{H^{\pm\pm}}, h_{XY}\}$ parameter plane after imposing the existing flavor bounds as well as different direct search limits. After pinning down the allowed region of the parameter space, we present the detailed analysis in section 3 for **3 TeV** muon collider. For present discussion, we focus on three signal events $\mu^+\mu^- \rightarrow \mu^+\mu^-$, $\mu^+\mu^- \rightarrow e^+e^-$ and $\mu^+\mu^- \rightarrow \tau^+\tau^-$ as these channels enable us to impose absolute bounds on $\{h_{\mu\mu}, h_{\mu e}, h_{\mu\tau}\}$ couplings respectively *w.r.t* doubly charged scalar mass. In section 4 we illustrate the corresponding reach plots in the aforementioned parameter plane. Before concluding our discussion, in section 5 we demonstrate a crucial aspect of this muon collider in terms of distinguishing two different NP scenarios. Finally, we summarize our study in section 6.

2 Setup

The interaction Lagrangian, which is relevant for our study, will take the following form:

$$\mathcal{L} \supset \sum_{i,j=e,\mu,\tau} h_{ij} e_L^{Ti} \mathcal{C} H^{++} e_L^j + \text{h.c.} \quad (1)$$

Here, the coefficient h_{ij} indicates leptonic couplings of the doubly charged scalar, and \mathcal{C} denotes the charge conjugation operator. This *phenomenological* choice of the Lagrangian term can be realized in various scalar extended BSM scenarios, for e.g., hybrid seesaw [87], Zee-Babu [88, 89] and left-right symmetric model [7–11, 17, 18] to name a few. Depending on the model, one can set the explicit value of h_{ij} and the doubly charged scalar mass $m_{H^{\pm\pm}}$. Instead of focusing on any specific model, we attempt to probe the above interaction maximally using the proposed muon collider. We find that the muon machine helps in imposing an absolute bound on the values of $h_{\mu\tau}, h_{\mu\mu}$ couplings, which are still missing in the literature. To emphasize this point, we present in Table 1, the different flavor-violating processes that could be influenced by the presence of a doubly charged scalar that couples to the charged leptons. The table includes constraints on the scalar’s couplings derived from these processes [90, 91]. It is worth noting that the flavor-changing decays such as $\ell_i \rightarrow \ell_j \ell_k \bar{\ell}_l$, where ℓ represent the charged leptons only, are absent in the SM. In contrast, these modes can emerge even at the tree-level in models with doubly charged scalars that allow flavor-violation in the leptonic decay modes. On the other hand, for processes like $\ell_i \rightarrow \ell_j \gamma$, that can arise within the SM at 1-loop via the W -boson exchange, one

Process	Experimental Bound	Constraint on	Bound $\times (m_{H^{\pm\pm}}/\text{TeV})^2$
$\mu \rightarrow e\gamma$	$< 4.2 \times 10^{-13}$ [92]	$ \sum_{k=e,\mu,\tau} h_{k\mu}^\dagger h_{ke} $	$< 2.4 \times 10^{-4}$
$\mu \rightarrow 3e$	$< 1.0 \times 10^{-12}$ [93]	$ h_{\mu e} h_{ee} $	$< 2.3 \times 10^{-5}$
$\tau \rightarrow e\gamma$	$< 3.3 \times 10^{-8}$ [94]	$ \sum_{k=e,\mu,\tau} h_{ke}^\dagger h_{k\tau} $	$< 1.6 \times 10^{-1}$
$\tau \rightarrow \mu\gamma$	$< 4.2 \times 10^{-8}$ [95]	$ \sum_{k=e,\mu,\tau} h_{k\mu}^\dagger h_{k\tau} $	$< 1.9 \times 10^{-1}$
$\tau \rightarrow 3e$	$< 2.7 \times 10^{-8}$ [96]	$ h_{\tau e} h_{ee} $	$< 9.2 \times 10^{-3}$
$\tau \rightarrow \mu^+ \mu^- e^-$	$< 2.7 \times 10^{-8}$ [96]	$ h_{\tau\mu} h_{\mu e} $	$< 6.5 \times 10^{-3}$
$\tau \rightarrow e^+ \mu^- \mu^-$	$< 1.7 \times 10^{-8}$ [96]	$ h_{\tau e} h_{\mu\mu} $	$< 7.3 \times 10^{-3}$
$\tau \rightarrow e^+ e^- \mu^-$	$< 1.8 \times 10^{-8}$ [96]	$ h_{\tau e} h_{\mu e} $	$< 5.3 \times 10^{-3}$
$\tau \rightarrow \mu^+ e^- e^-$	$< 1.5 \times 10^{-8}$ [96]	$ h_{\tau\mu} h_{ee} $	$< 6.9 \times 10^{-3}$
$\tau \rightarrow 3\mu$	$< 2.1 \times 10^{-8}$ [96]	$ h_{\tau\mu} h_{\mu\mu} $	$< 8.1 \times 10^{-3}$
$M \rightarrow \bar{M}$	$\leq 8.2 \times 10^{-11}$ [97]	$ h_{ee} h_{\mu\mu} $	$< 4.9 \times 10^{-2}$
$ee \rightarrow ee$ [LEP]	$\Lambda_{\text{eff}} > 5.2 \text{ TeV}$ [98]	$ h_{ee} ^2$	$< 1.2 \times 10^{-1}$
$ee \rightarrow \mu\mu$ [LEP]	$\Lambda_{\text{eff}} > 7.2 \text{ TeV}$ [98]	$ h_{\mu e} ^2$	$< 6.4 \times 10^{-2}$
$ee \rightarrow \tau\tau$ [LEP]	$\Lambda_{\text{eff}} > 7.6 \text{ TeV}$ [98]	$ h_{e\tau} ^2$	$< 5.4 \times 10^{-2}$

Table 1: The updated bounds on different flavor-violating as well as flavor conserving processes which were measured by different experimental collaborations. From the last column, one can notice that all these bounds depend on the underlying doubly charged scalar mass.

gets additional contributions from the doubly charged scalar that can modify the corresponding cross-section. Apart from these lepton flavor-violating processes, the Large Electron-Positron (LEP) collider facility also searched for doubly charged scalars in the $e^+e^- \rightarrow \ell_i^+ \ell_i^-$ channels. It is important to note that the majority of these abovementioned processes are primarily proportional to the multiplicative coupling factor $h_{ij} h_{kl}^*$, where each index represents the lepton families. As mentioned before, the muon collider provides us with the scope to probe to significant sensitivity, the individual $\{h_{\mu\tau}, h_{\mu\mu}, h_{\mu e}\}$ couplings that can be realized from the Feynman diagram illustrated in Figure 1, very similar to LEP which imposed absolute bounds on $\{h_{ee}, h_{e\mu}, h_{e\tau}\}$. One can always choose a fine-tuned value for the

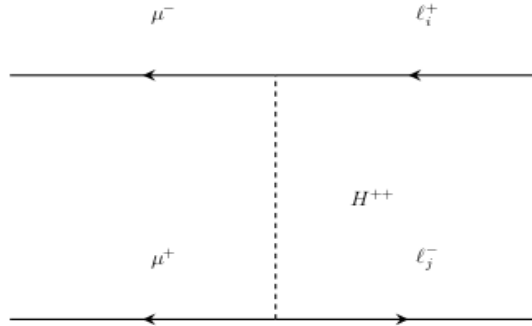


Figure 1: The t -channel Feynman diagram correspond to the $H^{\pm\pm}$ mediated signal process $\mu^+ \mu^- \rightarrow \ell_i^+ \ell_j^-$, where the index stands for $i, j = e, \mu, \tau$.

h_{ij} (where $i, j = e, \tau$) to satisfy these constraints while keeping the value of $\{h_{\mu\tau}, h_{\mu\mu}, h_{\mu e}\}$ at $\mathcal{O}(1)$.

To emphasize this point, let us consider the muonium-antimuonium transition $M \rightarrow \bar{M}$ [97]. Here, the upper bound on the probability of conversion between the LFV bound states (*i.e.* $\mu^+ e^- \longleftrightarrow \mu^- e^+$) will take the following form

$$\frac{|h_{ee} h_{\mu\mu}|}{(m_{H^{\pm\pm}}/\text{TeV})^2} \leq 4.9 \times 10^{-2}. \quad (2)$$

If we consider a BSM scenario which contains a doubly charged scalar of mass $m_{H^{\pm\pm}} = 1 \text{ TeV}$ and choose $h_{ee} = \mathcal{O}(10^{-3})$, then the corresponding value of $h_{\mu\mu}$ can be fixed at $\mathcal{O}(1)$ while respecting the relevant limit. Similarly, the $ee \rightarrow ee$ bound from LEP suggests that $|h_{ee}| < 0.346$ for the $m_{H^{\pm\pm}} = 1 \text{ TeV}$.

Using the given bounds in Table 1, we determine the excluded region in the parameter plane of $\{m_{H^{\pm\pm}}, h_{i\mu}\}$ (where $i = \mu, e, \tau$). In Figure 2 we present the maximum allowed value¹ of $h_{\mu i}$ (where $i = \mu, e, \tau$) with respect to doubly charged scalar mass $m_{H^{\pm\pm}}$. As expected, both the $h_{\mu\mu}$ and $h_{\mu\tau}$ can be $\mathcal{O}(1)$ without violating any low-energy experimental limits. In contrast, $h_{\mu e}$ has the strongest limit and is constrained to values less than $\mathcal{O}(1)$ for $m_{H^{\pm\pm}} \lesssim 4 \text{ TeV}$. This is expected as $ee \rightarrow \mu\mu$ scattering observed at LEP imposes an absolute bound on the coupling $h_{\mu e}$ while no such bound is available for the other two couplings.

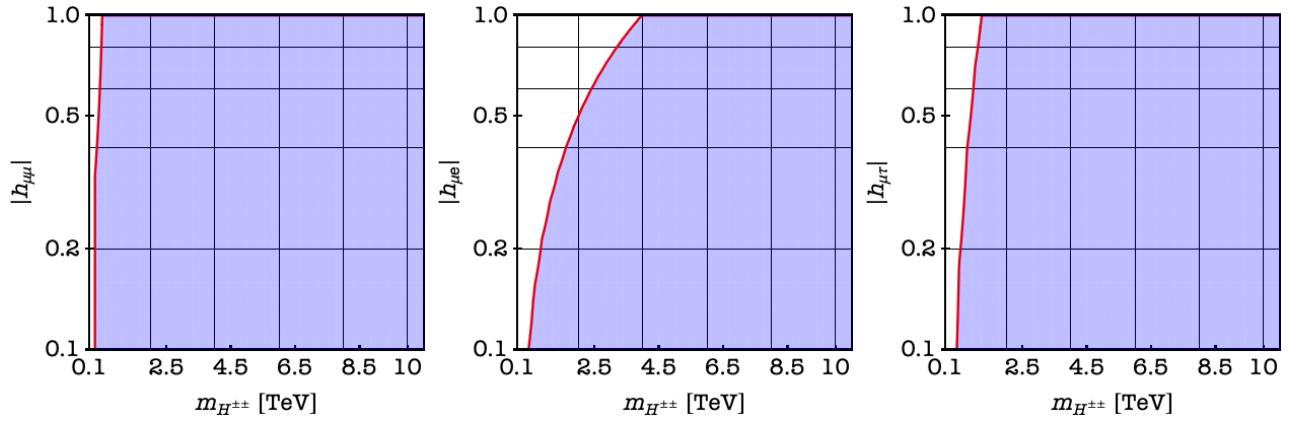


Figure 2: The allowed region in the $m_{H^{\pm\pm}}$ vs. $h_{\mu i}$ (where $i = \mu, e, \tau$) plane after simultaneously satisfying all relevant flavor data shown in Table 1. The Blue shaded region represent allowed region of the parameter space after imposing available flavor bounds.

Before concluding this section, we would like to point out that both ATLAS and CMS Collaborations have searched for these doubly charged scalars [27, 100] in the pure leptonic decay modes and found no significant excess after analyzing the Run 2 data. The null result of these analyses imposes a lower limit on $m_{H^{\pm\pm}}$, which is roughly around 1065 GeV from ATLAS in the LRSM case, irrespective of the leptonic final state. The analysis uses the pair production of the doubly charged scalar mediated by the neutral gauge bosons in the model. These limits are model dependent, and for example in the case of the Zee-Babu model [88], the lower limit is relaxed to 880 GeV due to the absence of the Z -mediated diagram.

¹To perform the scan on $h_{\mu i}$ we have fixed the upper bound $h_{\mu i} < 8\pi$. This choice is motivated from the perturbativity constraint [99].

$\tau^+\tau^-$	$Z\ell^+\ell^-$	$W\ell\nu$	$\ell^+\ell^-$
11.71 fb	57.17 fb	1.909 pb	13.25 pb

Table 2: SM background cross section at the muon collider with the c.o.m energy $\sqrt{s} = 3$ TeV.

3 Analysis

In this section, we provide a detailed analysis of the potential of a muon collider operating at $\sqrt{s} = 3$ TeV to thoroughly explore the $\{m_{H^{\pm\pm}}, h_{\mu i}\}$ parameter space. To do so, we consider three different signal topologies *i.e.* $\mu^+\mu^- \rightarrow e^+e^-$, $\mu^+\mu^- \rightarrow \mu^+\mu^-$ and $\mu^+\mu^- \rightarrow \tau^+\tau^-$ as illustrated in the Feynman diagram of Figure 1. The irreducible as well as reducible SM processes, which can make the search process challenging, are listed in the Table 2 along with their corresponding production rates at the muon collider. To analyze the strength of the cross-sections shown in Table 2, it is essential to examine the underlying subprocesses contributing to each. The $\tau\tau$ background arises primarily via an s -channel process, with its cross-section suppressed by the propagator (γ & Z) as $\sqrt{s} = 3$ TeV $\gg M_{Z,\gamma}$. The $Z\ell\ell$ and $W\ell\nu$ backgrounds, on the other hand, give reduced cross-sections due to a combination of phase space suppression and the involvement of additional α_{EW}/α_{em} in the $2 \rightarrow 3$ process. In contrast, the $\ell^+\ell^-$ can be generated through both s -channel (which is again suppressed due to reasons mentioned above) and t -channel diagrams. The t -channel contributions to the cross section are significant for small scattering angles and constitute the most substantial background in our analysis. To calculate the signal cross section, one can use the explicit formula [89] (neglecting the muon mass),

$$\left(\frac{d\sigma}{d\Omega}\right)_{\text{Fig.(1)}} = \left(\frac{h_{\mu i}^2}{4\pi}\right)^2 \frac{1}{s} \left[\frac{s^2 (1 + \cos\theta)^2}{(s + s \cos\theta + 2m_{H^{\pm\pm}}^2)^2} \right]. \quad (3)$$

Here, the label i can be varied depending on the final state leptons. The θ is angle between initial state μ^- and ℓ_i^- . To generate signal processes, we incorporate the interaction Lagrangian of Eq.(1) in FEYNRULESv2.3.x [101] and create the necessary UFO file. To estimate the cross-section for the signal and the SM backgrounds, we use MadGraph5@NL0v2.9.21 [102].

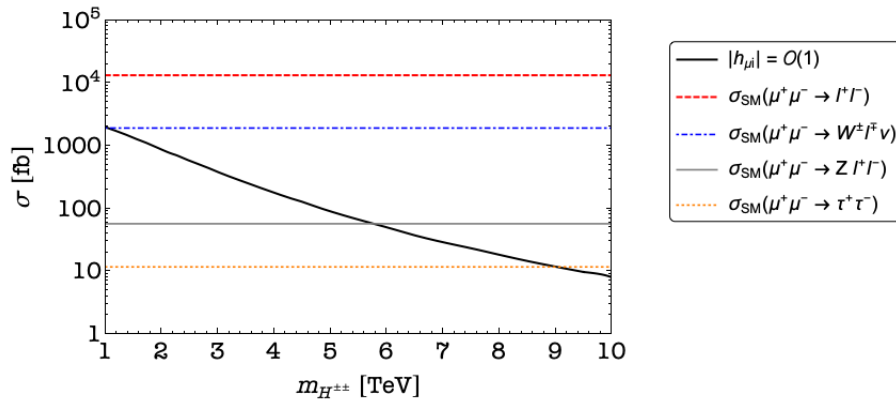


Figure 3: The cross section corresponds to both the signal and SM background processes generated at the muon collider at $\sqrt{s} = 3$ TeV. To calculate the signal cross section we have set the relevant vertex at $\mathcal{O}(1)$. The index i in $|h_{\mu i}|$ represents $i = e, \mu, \tau$ respectively.

In Figure 3 we present the cross-sections for the doubly charged scalar-mediated process by the black solid line as a function of the scalar mass. The SM background contributions are independent of the scalar mass and their values are constant for the given c.o.m. energy and are shown by the horizontal lines *viz.* $\ell^+\ell^-$ (red dashed line), $W^\pm\ell^\mp\nu$ (blue dot-dashed), $Z\ell^+\ell^-$ (gray solid line) and $\tau^+\tau^-$ (orange dotted line), respectively. The steady fall of the signal cross section can be understood from Eq.(3) where the corresponding σ scales approximately as $\sim \left(\frac{1}{m_{H^{\pm\pm}}^4}\right)$. Although the $\ell^+\ell^-$ background appears dominant, we note that the background contributes significantly only when the leptons do not change flavor. So at a muon collider, the large t -channel contribution exists exclusively for the $\mu^+\mu^-$ final state. In all other scenarios involving lepton flavor change between the initial and final states, it remains insignificant. To generate events for both signal and SM background using MadGraph5@NLO, we impose the following pre-selection cuts

$$|\eta(\ell)| < 3.0; \quad p_T(\ell) > 10 \text{ GeV}; \quad \Delta R_{\ell\ell} \geq 0.2 \quad (4)$$

After simulating the events, we pass them to PYTHIA8 [103], which helps include final state radiations (FSR) and generates event shapes and distributions of the final state events to be used in detector simulations. The detector simulation is performed using DELPHESv3.5.0 [104] with the help of the appropriate muon collider card [105]. For each of the signal, we try to identify suitable observables that would warrant us to devise a suitable cut, which in turn would help us to reject SM backgrounds maximally while affecting the signal numbers minimally. Finally, we use Eq.(5) to evaluate the significance of our proposed cut-flow chart [106].

$$\mathcal{Z} = (2\mathcal{L})^{\frac{1}{2}} \left[(\sigma_S + \sigma_B) \ln \left(1 + \frac{\sigma_S}{\sigma_B} \right) - \sigma_S \right]^{\frac{1}{2}} \quad (5)$$

Here \mathcal{Z} represents significance and \mathcal{L} is the integrated luminosity of the collider. The σ_S and σ_B represent the effective cross-section of the signal and background, respectively, after implementing all the cuts. In the following, we will present a detailed description of each final state separately.

3.1 $\mu^+\mu^-$ Channel

We begin our discussion with the $\mu^+\mu^-$ signal topology while selecting exactly two muons in the final state. We impose the following kinematic selection criteria on the final state muons:

$$p_T(\mu) > 50 \text{ GeV}; \quad |\eta(\mu)| < 2.4 \quad (6)$$

The cross section for the signal arising from the doubly charged scalar exchange is calculated with the scalar mass as $m_{H^{\pm\pm}} = 1250 \text{ GeV}$ and assuming the Yukawa coupling to be $h_{\mu\mu} = 1$. A quick look at Table 2 suggests that most of the SM background subprocesses ($W\ell\nu$, $\tau^+\tau^-$ and $Z\ell^+\ell^-$) will all contain neutrinos in the final states from their decay products, which give rise to missing energy (E_T^{miss}) in the final state events. In contrast, both the signal and $\ell^+\ell^-$ background do not have any direct source of missing energy.

In the *left* panel of Figure 4, we show the E_T^{miss} distribution, whereas the *right* panel illustrates the transverse momentum distribution of the leading muon, corresponding to both the signal and the relevant SM background processes. Note that, unlike the signal and $\ell^+\ell^-$ backgrounds, all the other backgrounds have a long tail in the missing energy distribution. Theoretically, for both the signal and $\ell^+\ell^-$ background, all the events must be concentrated in the bin with zero missing energy. However, due to the limitation in detector resolution efficiency, there is a finite mismeasurement probability

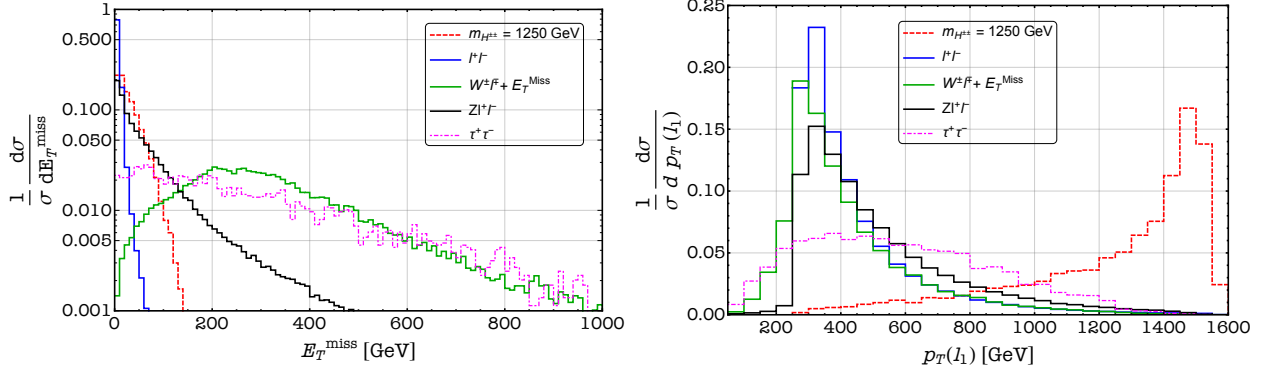


Figure 4: Normalized distribution of kinetic variables E_T^{miss} (left panel) and $p_T(\ell_1)$ (right panel) for both the signal and SM backgrounds for $\mu^+\mu^-$ final state.

that leads to a spread in missing energy distribution for both these processes as well. To restrict the SM background that contains neutrinos and lead to large missing energy in the event topology, we impose $E_T^{\text{miss}} < 100$ GeV to suppress their contributions. The effect of this cut becomes obvious as both the signal and $\ell^+\ell^-$ are marginally affected by this cut, while all the other SM backgrounds go down significantly. Table 3, illustrates the cut-flow chart for the signal-background analysis. Note that the E_T^{miss} cut hardly makes any improvement in the σ_S/σ_B ratio (last column in the table) since the dominant background for this final state comes from the SM di-lepton production that contains the $\mu^+\mu^-$ final state. The transverse momentum of the leading muon $p_T(\mu_1)$ becomes instrumental in suppressing this large background, as shown in the *right* panel of Figure 4. The leading muon's transverse momenta is seen to peak for large values (near 1450 GeV), whereas all the SM backgrounds peak for lower values and drop off around 1000 GeV. This is expected as the signal is mediated by a heavy propagator that leads to the final state leptons being produced more in the central rapidity region and therefore larger transverse momenta. On the other hand, for the dominant SM background arising from the t -channel exchange of photon and Z boson, which are effectively massless propagators compared to the c.o.m. energy, the final state leptons have a stronger probability of being produced at small scattering angles and therefore smaller transverse momenta. Exploiting this feature in $p_T(\mu_1)$ distribution, we impose a cut of $p_T(\mu_1) > 1350$ GeV² that helps improve the signal significance ~ 2.5 times when compared to the E_T^{miss} cut.

	$m_{H^{\pm\pm}} = 1250$ GeV	$\ell^+\ell^-$	$W\ell\nu$	$\tau^+\tau^-$	$Z\ell^+\ell^-$	$\frac{\sigma_S}{\sigma_B}$
$N_\mu = 2$	1.574×10^3	3.528×10^3	5.82×10^2	2.597	2.38	0.383
$E_T^{\text{miss}} < 100$ GeV	1.542×10^3	3.524×10^3	4.1×10^1	0.614	1.81	0.432
$p_T(\mu_1) > 1350$ GeV	7.84×10^2	20.0	0.0764	0	0.0142	39.02

Table 3: Benchmark analysis for the $\mu\mu$ final state. All the cross-sections presented in the above table are in fb. In the last column, we use the signal-to-background ratio ($\frac{\sigma_S}{\sigma_B}$) to represent the efficiency of each cut.

²Instead of $p_T(\mu_1)$ one could also use a cut on $|\eta_{\mu_1}|$ to achieve similar significance as both these variables are highly correlated. We have compared the effects of both these cuts separately and find that the $p_T(\mu_1)$ cut performs better.

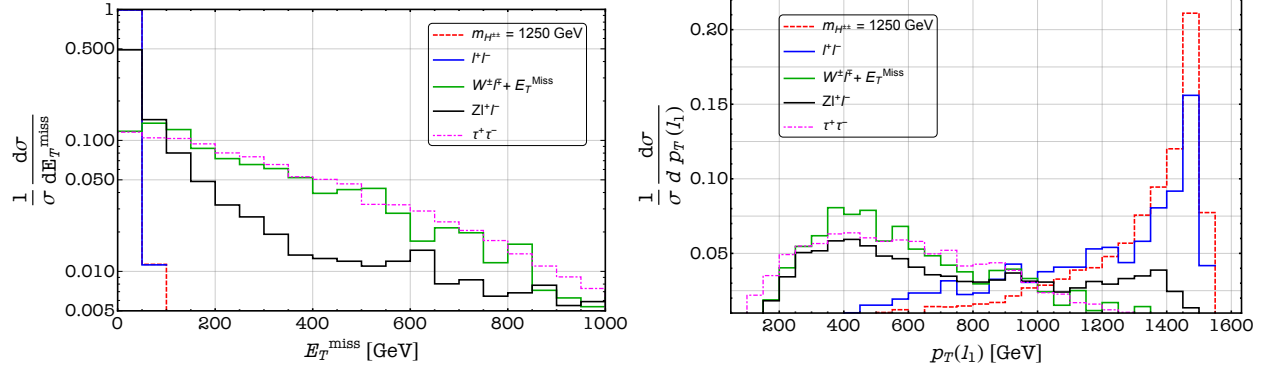


Figure 5: Normalized distribution of kinetic variables E_T^{miss} (left panel) and $p_T(\ell_1)$ (right panel) for both the signal and SM backgrounds for e^+e^- final state.

3.2 e^+e^- Channel

For the e^+e^- final state, we employ a similar strategy as described in the $\mu^+\mu^-$ case. However, after imposing $N_e = 2$ selection criteria, the dilepton background no longer receives contributions from the t -channel, as previously discussed. This renders the dilepton ($\mu^+\mu^- \rightarrow e^+e^-$) background very small due to the inherent s -channel suppression. This can be seen in Table 4 where, after demanding two electrons in the final state, the cross section of the $\ell^+\ell^-$ background reduces significantly. As before, we choose a similar selection cut for the outgoing electrons given by

$$p_T(e) > 50 \text{ GeV}, \quad |\eta(e)| < 2.4. \quad (7)$$

In Figure 5, we show the E_T^{miss} and $p_T(e_1)$ distributions for the signal and SM background processes. Similar to the case of the muon final states, all SM contributions exhibit significant events at large E_T^{miss} except for the di-lepton background. The signal and di-lepton background events are again concentrated within the 100 GeV bin. However, the missing transverse energy cut proves to be more effective for this final state, as the remaining dilepton background, being largely unaffected by this cut, is already minimal. Therefore, the overall cross-section for the SM background is significantly reduced by this cut. In Table 4, we show the cut flow chart for the e^+e^- final state. We first impose an upper bound on $E_T^{\text{miss}} < 50 \text{ GeV}$, which now enables us to achieve an improved σ_S/σ_B ratio. We observe that the $p_T(e_1)$ distribution for the di-lepton background is unlike the muon case, as it no longer has the substantial contributions from the t -channel process. Since the dominant production mechanism for the e^+e^- final state is an s -channel process, the outgoing fermions tend to be produced back-to-back in the central region, leading to a characteristic peak around half the c.o.m. energy, as illustrated in the figure. Fortunately, the dilepton background is small in this case, and therefore, the application of the cut $p_T(e_1) > 1300 \text{ GeV}$ significantly suppresses the remaining background contributions, effectively doubling the signal-to-background ratio.

3.3 $\tau^+\tau^-$ Channel

For the $\tau^+\tau^-$ final state, we adopt a different strategy owing to the challenges associated with the τ reconstruction. Here, for our analysis, we demand that both the τ in the final state must decay

	$m_{H^{\pm\pm}} = 1250 \text{ GeV}$	$\ell^+\ell^-$	$W\ell\nu$	$\tau^+\tau^-$	$Z\ell^+\ell^-$	$\frac{\sigma_S}{\sigma_B}$
$N_e = 2$	1.151×10^3	8.672	21.316	2.449	5.817×10^{-2}	35.81
$E_T^{\text{miss}} < 50 \text{ GeV}$	1.137×10^3	8.575	2.502	0.2831	2.858×10^{-2}	91.25
$p_T(e_1) > 1300 \text{ GeV}$	6.54×10^2	3.615	0.0382	5×10^{-4}	3.89×10^{-4}	178.91

Table 4: Benchmark analysis for the e^+e^- final state. All the cross-sections presented in the above table are in fb. In the last column, we use the signal-to-background ratio ($\frac{\sigma_S}{\sigma_B}$) to represent the efficiency of each cut.

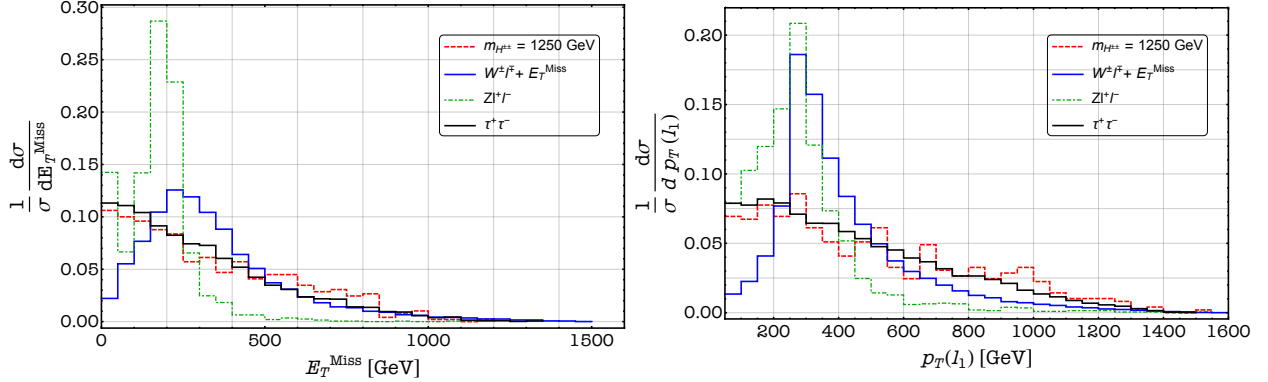


Figure 6: Normalized distribution of kinetic variables E_T^{miss} (left panel) and $p_T(\ell_1)$ (right panel) for both the signal and SM backgrounds for $\tau^+\tau^-$ final state.

via leptonic mode³. Among the three possible pure leptonic final states (*i.e.* $\mu^+\mu^- \rightarrow e^+e^- + E_T^{\text{miss}}$, $\mu^+\mu^- \rightarrow \mu^+\mu^- + E_T^{\text{miss}}$, $\mu^+\mu^- \rightarrow \mu^\pm e^\mp + E_T^{\text{miss}}$), we demand that the final state consists of $N_e = 1$ & $N_\mu = 1$, maintaining the kinematic requirements of Eq.(6) and Eq.(7). This allows us to avoid the dominant SM background associated with the t -channel dilepton production.

In Figure 6 we display the distributions corresponding to E_T^{miss} and $p_T(\ell_1)$ ⁴ for both the signal and the backgrounds. From the shape of the distributions, one can ascertain that there is no specific discriminating feature that can help in devising a cut to improve the signal significance. Interestingly, we find that the signal distributions in τ completely lose the characteristic peak in the transverse momentum that was observed for both the $\mu\mu$ and ee channels earlier, following a similar production mode. Hence, we consider alternative variables. As absolute energy variables do not seem to help our cause, we consider angular variables to check whether we find any distinguishing features between the signal and SM backgrounds. In Figure 7 we show the distributions in $\Delta R_{\ell\ell}$, which measures the angular separation between the two outgoing leptons, and $|\cos\theta_\mu|$ which represents the angle of the μ -tagged lepton with the beam axis, for the signal and SM background events. We observe that the variable $\Delta R_{\ell\ell}$ exhibits a pronounced peak for both the signal and the $\tau^+\tau^-$ background, whereas other background processes show a more uniform distribution across the full range. Additionally, the event shape of the absolute value of the complementary variable $|\cos\theta_\mu|$ reveals that the $W\ell\nu$ and $Z\ell^+\ell^-$ backgrounds predominantly peak in the 0.9 to 1.0 bin as opposed to the signal and the $\tau^+\tau^-$ background. This motivates the application of the selection cut $|\cos\theta_\mu| < 0.8$ to suppress these backgrounds, further improving the signal-to-background ratio. In Table 5, we present the details of

³One can also choose hadronic decays of the τ . However, in that scenario, one must also account for an additional set of jet-associated SM background.

⁴We wish to point out that in this case leading lepton can be either electron or muon.

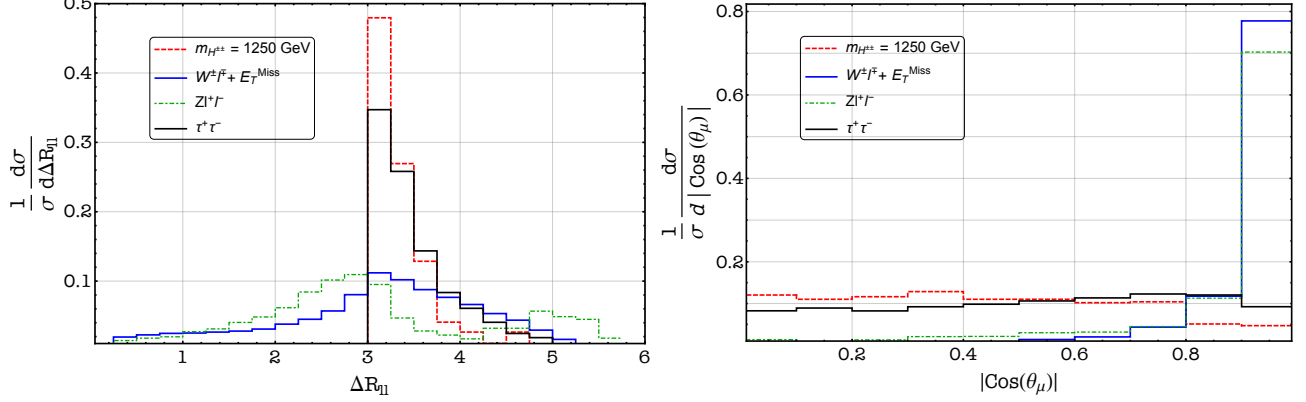


Figure 7: Normalized distribution of kinetic variables $\Delta R_{\ell\ell}$ (left panel) and $\cos\theta_\mu$ (right panel) for both the signal and SM backgrounds for $\tau^+\tau^-$ final state.

	$m_{H^{\pm\pm}} = 1250 \text{ GeV}$	$W\ell\nu$	$\tau^+\tau^-$	$Z\ell^+\ell^-$	$\frac{\sigma_S}{\sigma_B}$
$N_e = 1 \ \& \ N_\mu = 1$	7.36×10^1	5.35×10^2	5.37	2.31×10^{-2}	0.136
$ \cos\theta_\mu < 0.8$	6.63×10^1	5.61×10^1	4.22	4.26×10^{-3}	1.097

Table 5: Benchmark analysis for the $\tau\tau$ final state. All the cross-sections presented in the above table are in fb.

the cut and count analysis.

4 Results

We now demonstrate how the muon collider with $\sqrt{s} = 3 \text{ TeV}$, using the three final state topologies $\mu^+\mu^-$, e^+e^- and $\tau^+\tau^-$, improves our sensitivity reach for the mass and leptonic couplings of the doubly-charged scalar. The obtained results, following the methodology discussed in the previous section, enable us to determine the maximum sensitivity reach for each Yukawa coupling involving the doubly charged scalar. The sensitivity plots for the three cases analyzed in the previous section in the coupling-mass plane of the parameter space are shown in Figures 8, 9 and 10. For the sensitivity plots, we have chosen an integrated luminosity $\mathcal{L} = 1000 \text{ fb}^{-1}$. We discuss below our findings in each of the sensitivity plots.

- $\mu^+\mu^- \rightarrow \mu^+\mu^-$:

We have previously outlined the event selection criteria to enhance signal significance for the $\mu^+\mu^-$ final state. Since the signal cross section was initially generated assuming $h_{\mu\mu} = 1$, it can be straightforwardly rescaled for any given value of $|h_{\mu\mu}|$ corresponding to different scalar mass choices. The variation of the signal cross section with respect to the scalar mass is already shown in Figure 3. In Figure 8, we illustrate the parameter space in the $m_{H^{\pm\pm}}, |h_{\mu\mu}|$ plane that can be probed using the cut-flow strategy detailed in Table 3. The *dark green* and *dark magenta* shaded regions represent the areas where a statistical significance exceeding 2σ and 5σ , respectively, can be achieved. The *light-red* vertical bar represents the direct search limit from LHC ($m_{H^{\pm\pm}} \lesssim 1100 \text{ GeV}$) extracted from the ATLAS analysis [100]. It is evident from the figure that

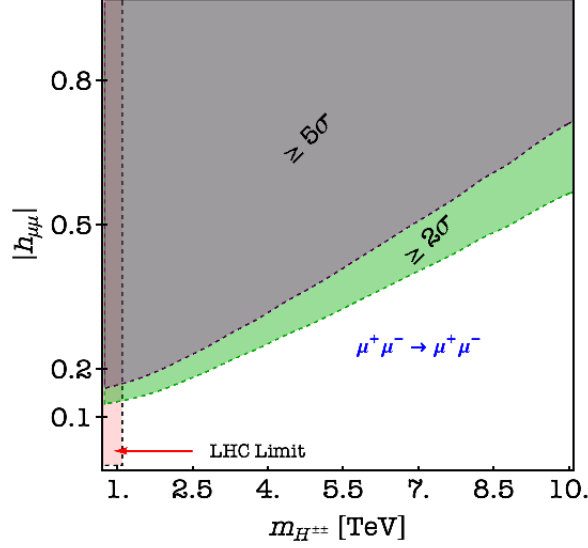


Figure 8: Illustrating the sensitivity reach for $|h_{\mu\mu}|$ as a function of the doubly charged scalar mass following the cut and count analysis described in section 3, for an integrated luminosity $\mathcal{L} = 1000 \text{ fb}^{-1}$ and $\sqrt{s} = 3 \text{ TeV}$.

our analysis substantially extends the discovery reach for the doubly charged scalar mass $m_{H^{\pm\pm}}$, from the current exclusion limit on $m_{H^{\pm\pm}}$, for Yukawa couplings in the range $|h_{\mu\mu}| \approx 0.15$ to $|h_{\mu\mu}| \approx 0.65$. In fact, no direct limits on the $h_{\mu\mu}$ coupling exist in the literature, and the muon collider will provide an exclusive opportunity to probe this coupling to very small values for an extended range of doubly charged scalar mass beyond the reach of LHC and lepton-flavor-violation experiments.

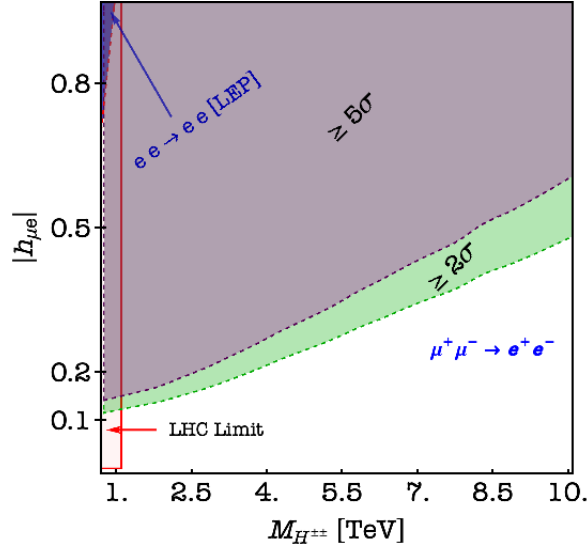


Figure 9: Illustrating the sensitivity reach for $|h_{\mu e}|$ as a function of the doubly charged scalar mass following the cut and count analysis described in section 3, for an integrated luminosity $\mathcal{L} = 1000 \text{ fb}^{-1}$ and $\sqrt{s} = 3 \text{ TeV}$.

- $\mu^+\mu^- \rightarrow e^+e^-$:

In this channel, the contribution to the signal comes through the t -channel exchange of the doubly charged scalar, and the vertex violates lepton flavor. This process, therefore, corresponds to the flavor-violating vertex $h_{\mu e}$. In Figure 9 we illustrate the region in the parameter plane $\{m_{H^{\pm\pm}}, |h_{\mu e}|\}$ which can be probed using the cut-flow chart discussed in Table. (4). The *dark green* and *dark magenta* shaded regions in the plot indicate areas of the parameter space that can be probed with statistical significances exceeding 2σ and 5σ , respectively. Additionally, the *dark blue* shaded area in the upper-left corner corresponds to the $e^+e^- \rightarrow e^+e^-$ constraint from LEP, as summarized in Table 1. The *light red* shaded region represents the existing LHC limit, as discussed previously. The reach plot suggest that, one can probe the $m_{H^{\pm\pm}}$ in the 1.1 TeV to 10 TeV range for the corresponding $h_{\mu e} \approx 0.1$ to $h_{\mu e} \approx 0.41$. When compared with current experimental bounds, the reach of our analysis represents a substantial improvement over both collider and flavor experiments.

- $\mu^+\mu^- \rightarrow \tau^+\tau^-$:

Finally, we comment on the significance of the $\tau^+\tau^-$ final state in probing the flavor violating $h_{\mu\tau}$ coupling. In Figure 10 we show the region of the parameter plane $\{m_{H^{\pm\pm}}, |h_{\mu\tau}|\}$ which can be explored following the cut flow chart described in Table 5. For this signal topology, the most stringent available bound is from LHC, which is illustrated as *light-red* vertical bar. In this case as well, we show the 2σ and (*dark-green*) 5σ (*dark-magenta*) discovery contours, respectively. Compared to the previous two scenarios ($\mu\mu$ and ee), both the exclusion and discovery mass reaches are noticeably lower and reach values of $m_{H^{\pm\pm}} \lesssim 8$ TeV at 2σ and $m_{H^{\pm\pm}} \lesssim 6$ TeV at 5σ for $h_{\mu\tau} \approx \mathcal{O}(1)$. This is because of the challenges in τ identification, which significantly reduces the signal events. Notwithstanding this fact, the muon collider will still be able to probe

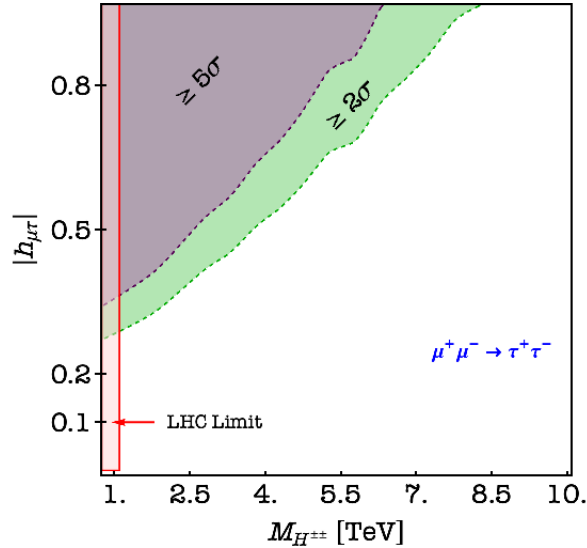


Figure 10: Illustrating the sensitivity reach for $|h_{\mu\tau}|$ as a function of the doubly charged scalar mass following the cut and count analysis described in section 3, for an integrated luminosity $\mathcal{L} = 1000 \text{ fb}^{-1}$ and $\sqrt{s} = 3 \text{ TeV}$.

the $h_{\mu\tau}$ coupling and the corresponding mass of the doubly charged scalar beyond any other foreseeable experiment.

5 Resolving a possible Inverse Problem

Before summarizing our primary findings, we would like to highlight an interesting possibility regarding the leptonic channels under consideration. As charge conservation is implicit, the analyzed final states can appear in several different incarnations of a BSM scenario. Of the many likely options of different spin particles contributing to the same process, the most notable option to highlight here would be the exchange of the neutral scalar that could mediate the processes in the same way as the doubly charged scalar. As the spin of the exchanged mediator has the knack of showing up through characteristic angular dependence in the final state particles, the challenge is more pronounced if we consider the same spin particle as an alternative. The central question is whether a muon collider possesses the capability to distinguish between different underlying scenarios, a challenge that lies at the heart of the *inverse problem* in particle physics.

To elaborate this, let us consider an alternative BSM scenario where a \mathbf{CP} -even heavy neutral scalar H^0 can give rise to identical signal topology $\mu^+\mu^- \rightarrow \ell_i^+\ell_j^-$ instead of a doubly charged scalar which we have considered above. The interaction Lagrangian for this substitute new physics model takes a very similar form to what we consider for the doubly charged scalar in Eq. (1), given as

$$\mathcal{L}_{H^0} \supset \sum_{i,j=e,\mu,\tau} \tilde{h}_{ij} \bar{\ell}_i H^0 \ell_j. \quad (8)$$

Here, all the fields are expressed in the mass basis, and the coefficient \tilde{h}_{ij} represents the coupling strength of the \mathbf{CP} -even neutral scalar H^0 with the SM charged leptons. Based upon the model, one can write down the explicit form of the leptonic coupling \tilde{h}_{ij} , which is a function of different parameters of the underlying model. For example, in case of Type-I 2HDM [99], the coupling $\tilde{h}_{ii} = \frac{m_{\ell_i}}{v} \cot \beta$ (the parameter β signifies the ratio between two *vev*'s of the model) and the coupling \tilde{h}_{ij} with $i \neq j$ is zero as the model does not allow FCNC. The interaction term of Eq.(8) can give rise to $\mu^+\mu^- \rightarrow \ell_i^+\ell_j^-$ processes and the corresponding Feynman diagrams are shown in Figure 11. From these diagrams, it is obvious that the final state arising from the neutral scalar-mediated process closely resembles that of the $H^{\pm\pm}$ -mediated process. (see Figure 1 for comparison). In this situation, one can ask the following

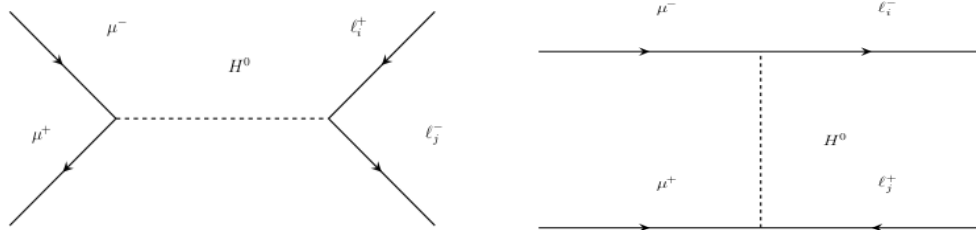


Figure 11: Illustrating the s - and t -channel Feynman diagrams corresponding to the H^0 mediated signal process $\mu^+\mu^- \rightarrow \ell_i^+\ell_j^-$, where the index $i, j = e, \mu, \tau$.

question -

Suppose after analyzing the $\mu^+\mu^- \rightarrow \mu^+\mu^-$ final state in the future muon collider one observe significant excesses of events *w.r.t* the SM background. Given the circumstances, can one infer

the nature of the underlying new physics (in this case, whether the excess is from a neutral or doubly charged scalar) responsible for the excess?

This is a crucial argument in what is termed as the “*Inverse problem*” and efforts exist [107] to address such questions in the context of future e^+e^- collider. Before introducing a discriminating variable aimed at resolving this issue, we would like to underscore the differences between Figure 1 and Figure 11, respectively. As opposed to the doubly charged scalar-mediated process involving $H^{\pm\pm}$, the neutral scalar scenario includes an s -channel mediated contribution. The presence of this diagram can substantially contribute to the corresponding cross-section. However, if one considers a neutral scalar mass m_{H^0} that is sufficiently far away from the c.o.m energy of the collider, then one can safely ignore its contributions. Under this premise, we are now in a position to compare two t – *channel* processes (see Figure 1 and *left* panel of Figure 11) which emerge from two distinct model hypothesis $\mathcal{L}_{H^{\pm\pm}}$ (see Eq.(1)) and \mathcal{L}_{H^0} (see Eq.(8)), respectively. The striking distinction between these two diagrams is that, for the $H^{\pm\pm}$ mediated process, there is a charge flip in the final state muon leg, which does not occur in the case of the heavy neutral scalar H^0 . This feature arises due to the presence of the charge conjugation operator in the $\mathcal{L}_{H^{\pm\pm}}$ Lagrangian. This aspect acts as the *de facto* rationale to build up the observable, which in turn will answer the problem in hand.

To address the aforementioned question, we simulate the $\mu^+\mu^- \rightarrow \mu^+\mu^-$ final state for these two different *new physics* scenarios separately using **MadGraph5@NL0**. We set the corresponding masses and couplings as $m_{H^{\pm\pm}} = m_{H^0} = 1250$ GeV and $h_{\mu\mu} = \tilde{h}_{\mu\mu} = \mathcal{O}(1)$ ⁵. To analyze both these signals,

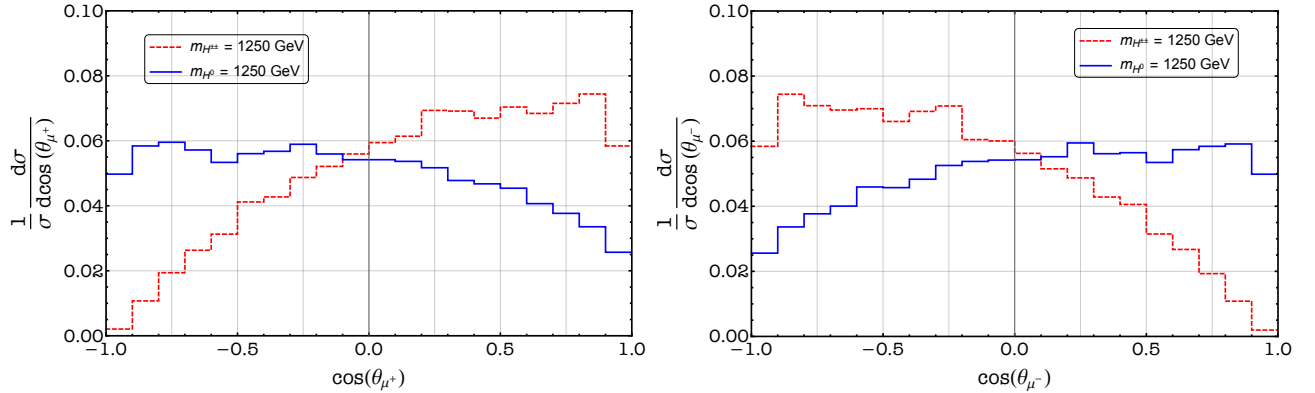


Figure 12: Normalized distribution of angular variables $\cos(\theta_{\mu+})$ (left panel) and $\cos(\theta_{\mu-})$ (right panel) for two different hypothesis $\mathcal{L}_{H^{\pm\pm}}$ and \mathcal{L}_{H^0} respectively.

we demand, emphasizing the charge identification of the muon, that $N_{\mu+} = N_{\mu-} = 1$, using the criteria given in Eq.(6). Our goal here is to construct a detectable observable that can enable us to distinguish between these two different new physics signals. To do so, we take into account the charge flipping of the final state muon leg, which happens for the doubly charged scalar scenario. As a result, one can think of angular variables $\cos(\theta_{\mu+})$ and $\cos(\theta_{\mu-})$. The corresponding distributions for these variables are presented in Figure 12. In case of $\cos(\theta_{\mu+})$ distribution, one can notice that for the doubly charged case, the events are monotonously increasing over the range $[-1, 1]$. In contrast, for the neutral scalar case, the events is monotonously decreasing over the range $[-1, 1]$. For $\cos(\theta_{\mu-})$ distribution, these

⁵Here we demand both these couplings $h_{\mu\mu}, \tilde{h}_{\mu\mu}$ are $\mathcal{O}(1)$. To achieve that coupling strength, one needs to ensure that the neutral and the doubly charged scalar do not belong to the same scalar multiplet. This restriction arises from the hypercharge assignment of the scalar multiplet

feature is completely opposite. For a quantitative measurement, we define two asymmetry variables \mathcal{A}_{\pm} whose explicit form is written in Eq. (12).

$$\mathcal{A}_{\pm}^{\text{NP}} = \frac{\left. \frac{d\sigma}{d\cos(\theta_{\mu\pm})} \right|_{\text{range}=[-1,0]} - \left. \frac{d\sigma}{d\cos(\theta_{\mu\pm})} \right|_{\text{range}=[0,1]}}{\left. \frac{d\sigma}{d\cos(\theta_{\mu\pm})} \right|_{\text{range}=[-1,1]}} \quad (9)$$

This variable can be effectively used to distinguish between the two scenarios, as it will yield numerical values that differ in their absolute sign, providing a clear and robust means of discrimination. In Table 6, we present the measure of the asymmetry parameter \mathcal{A}_{\pm} for the models $\mathcal{L}_{H^{\pm\pm}}$ and \mathcal{L}_{H^0} , respectively. As argued earlier, the sign of the measure plays the role of a discriminant between the two scenarios. For example, in the case of a doubly charged scalar $H^{\pm\pm}$, the \mathcal{A}_{+} takes a negative value as opposed to the neutral Higgs scenario. We have therefore identified and proposed a crucial variable that could

Model Type	Benchmark	\mathcal{A}_{+}	\mathcal{A}_{-}
$\mathcal{L}_{H^{\pm\pm}} \rightarrow \text{Eq. (1)}$	$m_{H^{\pm\pm}} = 1250 \text{ GeV} \ \& \ h_{\mu\mu} = 1$	≈ -0.339	≈ 0.339
$\mathcal{L}_{H^0} \rightarrow \text{Eq. (8)}$	$m_{H^0} = 1250 \text{ GeV} \ \& \ \tilde{h}_{\mu\mu} = 1$	≈ 0.233	≈ -0.23

Table 6: The measure of asymmetry parameters \mathcal{A}_{\pm} are listed for the two different models $\mathcal{L}_{H^{\pm\pm}}$ and \mathcal{L}_{H^0} , respectively.

play a pivotal role in distinguishing the same spin particles of different electric charge through an asymmetry. This can also be used for other spin particles mediating similar final states and could be useful at future lepton colliders, including the ILC and CLIC.

6 Summary and Conclusion

In this work, we probe the strength of leptonic couplings of a doubly charged scalar at the future muon collider. These exotic scalars naturally appear in different BSM scenarios where the SM scalar spectrum is extended with at least one $\mathbf{Y} = 2$ non-trivial multiplet. In general, these models can accommodate non-zero neutrino masses, and as a consequence, the doubly charged scalars can couple to SM charged leptons with sizable strength. However, rather than restricting ourselves to a specific NP scenario, we adopt a model *agnostic* approach by extending the SM Lagrangian with relevant interaction terms. Much like the LEP collider, the proposed muon collider can probe these leptonic couplings in an absolute sense, i.e. it can individually constrain couplings such as $|h_{\mu e}|$, $|h_{\mu\mu}|$, and $|h_{\mu\tau}|$ by analyzing ee , $\mu\mu$, and $\tau\tau$ final states, respectively. Our analysis is performed for a muon collider operating at a center-of-mass energy of 3 TeV with an integrated luminosity of 1 ab^{-1} . By carefully analyzing the signal and the relevant SM background, we devise a suitable set of rectangular cuts that can suppress the dominant SM background while minimally affecting the signal strength. Using these optimized cuts, we evaluate the signal significance for doubly charged scalar masses in the range of 1 TeV to 10 TeV. Using the obtained signal significances, we further extract the discovery reach, presented in the plane of coupling versus mass, where we show that the muon collider can probe a significantly large region of parameter space compared to the existing bounds from flavor experiments and collider searches. The proposed limit on the absolute value of $|h_{\mu\mu}|$, and $|h_{\mu\tau}|$ would enrich the existing flavor bounds.

We also note that similar signals can arise from the t -channel exchange of a neutral scalar. However, by studying the angular distribution of the final-state leptons with respect to the muon beam axis, it is possible to discriminate between the doubly charged scalar and the neutral scalar hypotheses. In particular, we find that one can construct a forward-backward (FB) asymmetry variable

that exhibits characteristic features: a positive asymmetry score indicating a doubly charged scalar, while a negative score hints towards a neutral scalar.

Thus, a muon collider can offer an optimal environment not only to probe specific second-generation lepton flavor-violating couplings of doubly charged scalars but also to distinguish their effects from those of neutral scalar exchange processes. We would like to reiterate that the primary reason this collider can probe the mass scale of NP beyond that of the LHC, and which is much above the c.o.m energy of that collider, is because the doubly charged scalar can be produced via a t -channel process. This feature of the production mechanism can also be extended to other new physics scenarios, such as Z' , leptoquarks, and flavor-violating spin-2 particles. These possibilities provide additional motivation for the construction of a muon collider, which could significantly enhance the scope of future BSM investigations.

Acknowledgement

The work of NG was supported by the Japan Society for the Promotion of Science (JSPS) as a part of the JSPS Postdoctoral Program (Standard), grant number: JP24KF0189, and by the World Premier International Research Center Initiative (WPI), MEXT, Japan (Kavli IPMU). NG would also like to thank the Centre for High Energy Physics (CHEP), Indian Institute of Science (IISc), for financial support, where part of the work was done. A.S. thanks Anusandhan National Research Foundation (ANRF) for providing the necessary financial support through the SERB-NPDF grant (Ref No: PDF/2023/002572). S.K.R. acknowledges the support from the Department of Atomic Energy (DAE), India, for the Regional Centre for Accelerator-based Particle Physics (RECAPP), Harish Chandra Research Institute. AS would also like to thank Dr. Siddharth P. Maharathy for providing useful suggestions on the event simulation portion of the work.

References

- [1] **ATLAS** Collaboration, G. Aad et al., *Observation of a new particle in the search for the Standard Model Higgs boson with the ATLAS detector at the LHC*, *Phys. Lett. B* **716** (2012) 1–29, [[arXiv:1207.7214](#)].
- [2] **CMS** Collaboration, S. Chatrchyan et al., *Observation of a New Boson at a Mass of 125 GeV with the CMS Experiment at the LHC*, *Phys. Lett. B* **716** (2012) 30–61, [[arXiv:1207.7235](#)].
- [3] D. A. Ross and M. J. G. Veltman, *Neutral Currents in Neutrino Experiments*, *Nucl. Phys. B* **95** (1975) 135–147.
- [4] J. F. Gunion, R. Vega, and J. Wudka, *Higgs triplets in the standard model*, *Phys. Rev. D* **42** (1990) 1673–1691.
- [5] T. Nomura and H. Okada, *Muon $g - 2$ with $SU(2)_L$ multiplets**, *Chin. Phys. C* **49** (2025), no. 4 043102, [[arXiv:2208.08704](#)].
- [6] M. Magg and C. Wetterich, *Neutrino Mass Problem and Gauge Hierarchy*, *Phys. Lett. B* **94** (1980) 61–64.
- [7] G. Senjanovic and R. N. Mohapatra, *Exact Left-Right Symmetry and Spontaneous Violation of Parity*, *Phys. Rev. D* **12** (1975) 1502.

- [8] R. N. Mohapatra and J. C. Pati, *A Natural Left-Right Symmetry*, *Phys. Rev. D* **11** (1975) 2558.
- [9] R. N. Mohapatra and G. Senjanovic, *Neutrino Mass and Spontaneous Parity Nonconservation*, *Phys. Rev. Lett.* **44** (1980) 912.
- [10] N. G. Deshpande, J. F. Gunion, B. Kayser, and F. I. Olness, *Left-right symmetric electroweak models with triplet Higgs*, *Phys. Rev. D* **44** (1991) 837–858.
- [11] B. Brahmachari, E. Ma, and U. Sarkar, *Truly minimal left right model of quark and lepton masses*, *Phys. Rev. Lett.* **91** (2003) 011801, [[hep-ph/0301041](#)].
- [12] E. Ma, *Verifiable radiative seesaw mechanism of neutrino mass and dark matter*, *Phys. Rev. D* **73** (2006) 077301, [[hep-ph/0601225](#)].
- [13] R. N. Mohapatra, *Left-right Symmetry and Finite One Loop Dirac Neutrino Mass*, *Phys. Lett. B* **201** (1988) 517–524.
- [14] S. Saad, *Simplest Radiative Dirac Neutrino Mass Models*, *Nucl. Phys. B* **943** (2019) 114636, [[arXiv:1902.07259](#)].
- [15] B. S. Balakrishna and R. N. Mohapatra, *Radiative Fermion Masses From New Physics at TeV Scale*, *Phys. Lett. B* **216** (1989) 349–352.
- [16] P.-H. Gu and U. Sarkar, *Radiative Neutrino Mass, Dark Matter and Leptogenesis*, *Phys. Rev. D* **77** (2008) 105031, [[arXiv:0712.2933](#)].
- [17] S. P. Maharathy, M. Mitra, and A. Sarkar, *An alternate left-right symmetric model with Dirac neutrinos*, *Eur. Phys. J. C* **83** (2023), no. 6 480, [[arXiv:2211.09675](#)].
- [18] Z. A. Borboruah, L. Malhotra, U. Patel, S. Patra, and S. U. Sankar, *Left-Right Symmetric Neutrino Mass Model without Scalar Bi-doublet*, [[arXiv:2504.08267](#)].
- [19] **ATLAS** Collaboration, G. Aad et al., *Search for doubly-charged Higgs bosons in like-sign dilepton final states at $\sqrt{s} = 7$ TeV with the ATLAS detector*, *Eur. Phys. J. C* **72** (2012) 2244, [[arXiv:1210.5070](#)].
- [20] **ATLAS** Collaboration, G. Aad et al., *Search for anomalous production of prompt same-sign lepton pairs and pair-produced doubly charged Higgs bosons with $\sqrt{s} = 8$ TeV pp collisions using the ATLAS detector*, *JHEP* **03** (2015) 041, [[arXiv:1412.0237](#)].
- [21] **ATLAS** Collaboration, M. Aaboud et al., *Search for doubly charged Higgs boson production in multi-lepton final states with the ATLAS detector using proton–proton collisions at $\sqrt{s} = 13$ TeV*, *Eur. Phys. J. C* **78** (2018), no. 3 199, [[arXiv:1710.09748](#)].
- [22] **ATLAS** Collaboration, M. Aaboud et al., *Search for doubly charged scalar bosons decaying into same-sign W boson pairs with the ATLAS detector*, *Eur. Phys. J. C* **79** (2019), no. 1 58, [[arXiv:1808.01899](#)].
- [23] **ATLAS** Collaboration, G. Aad et al., *Search for doubly and singly charged Higgs bosons decaying into vector bosons in multi-lepton final states with the ATLAS detector using proton-proton collisions at $\sqrt{s} = 13$ TeV*, *JHEP* **06** (2021) 146, [[arXiv:2101.11961](#)].

- [24] **CMS Collaboration**, S. Chatrchyan et al., *A Search for a Doubly-Charged Higgs Boson in pp Collisions at $\sqrt{s} = 7$ TeV*, *Eur. Phys. J. C* **72** (2012) 2189, [[arXiv:1207.2666](#)].
- [25] **CMS Collaboration**, V. Khachatryan et al., *Study of vector boson scattering and search for new physics in events with two same-sign leptons and two jets*, *Phys. Rev. Lett.* **114** (2015), no. 5 051801, [[arXiv:1410.6315](#)].
- [26] **CMS Collaboration**, CMS Collaboration, *Search for a doubly-charged Higgs boson with $\sqrt{s} = 8$ TeV pp collisions at the CMS experiment*, .
- [27] **CMS Collaboration**, CMS Collaboration, *A search for doubly-charged Higgs boson production in three and four lepton final states at $\sqrt{s} = 13$ TeV*, .
- [28] **CMS Collaboration**, A. M. Sirunyan et al., *Observation of electroweak production of same-sign W boson pairs in the two jet and two same-sign lepton final state in proton-proton collisions at $\sqrt{s} = 13$ TeV*, *Phys. Rev. Lett.* **120** (2018), no. 8 081801, [[arXiv:1709.05822](#)].
- [29] S. Ashanujjaman and K. Ghosh, *Revisiting type-II see-saw: present limits and future prospects at LHC*, *JHEP* **03** (2022) 195, [[arXiv:2108.10952](#)].
- [30] **ECFA/DESY LC Physics Working Group Collaboration**, J. A. Aguilar-Saavedra et al., *TESLA: The Superconducting electron positron linear collider with an integrated x-ray laser laboratory. Technical design report. Part 3. Physics at an $e^+ e^-$ linear collider*, [hep-ph/0106315](#).
- [31] **Linear Collider American Working Group Collaboration**, T. Abe et al., *Linear Collider Physics Resource Book for Snowmass 2001 - Part 2: Higgs and Supersymmetry Studies*, in *APS / DPF / DPB Summer Study on the Future of Particle Physics*, 5, 2001. [hep-ex/0106056](#).
- [32] **Linear Collider ACFA Working Group Collaboration**, K. Abe et al., *Particle physics experiments at JLC*, [hep-ph/0109166](#).
- [33] A. Arbey et al., *Physics at the $e^+ e^-$ Linear Collider*, *Eur. Phys. J. C* **75** (2015), no. 8 371, [[arXiv:1504.01726](#)].
- [34] **CLIC Physics Working Group Collaboration**, E. Accomando et al., *Physics at the CLIC multi-TeV linear collider*, in *11th International Conference on Hadron Spectroscopy*, CERN Yellow Reports: Monographs, 6, 2004. [hep-ph/0412251](#).
- [35] **Linear Collider Vision Collaboration**, D. Attié et al., *A Linear Collider Vision for the Future of Particle Physics*, [arXiv:2503.19983](#).
- [36] **ILC Collaboration**, Baer, Howard and ILC Collaborations, *The International Linear Collider Technical Design Report - Volume 2: Physics*, [arXiv:1306.6352](#).
- [37] **Linear Collider Collaboration**, C. Balazs et al., *The Linear Collider Facility (LCF) at CERN*, [arXiv:2503.24049](#).
- [38] R. Godbole, B. Mukhopadhyaya, and M. Nowakowski, *Triplet Higgs bosons at $e^+ e^-$ colliders*, *Phys. Lett. B* **352** (1995) 388–393, [[hep-ph/9411324](#)].
- [39] K.-m. Cheung, R. J. N. Phillips, and A. Pilaftsis, *Signatures of Higgs triplet representations at TeV $e^+ e^-$ colliders*, *Phys. Rev. D* **51** (1995) 4731–4737, [[hep-ph/9411333](#)].

- [40] C.-W. Chiang, S. Kanemura, and K. Yagyu, *Phenomenology of the Georgi-Machacek model at future electron-positron colliders*, *Phys. Rev. D* **93** (2016), no. 5 055002, [[arXiv:1510.06297](#)].
- [41] K. Yagyu, *Doubly-charged Higgs bosons in the diboson decay scenario at the ILC*, in *International Workshop on Future Linear Colliders*, 5, 2014. [arXiv:1405.5149](#).
- [42] X.-H. Bai, Z.-L. Han, Y. Jin, H.-L. Li, and Z.-X. Meng, *Same-sign tetralepton signature in type-II seesaw at lepton colliders*, *Chin. Phys. C* **46** (2022), no. 1 012001, [[arXiv:2105.02474](#)].
- [43] S. Blunier, G. Cottin, M. A. Díaz, and B. Koch, *Phenomenology of a Higgs triplet model at future e^+e^- colliders*, *Phys. Rev. D* **95** (2017), no. 7 075038, [[arXiv:1611.07896](#)].
- [44] N. Kumar, *Unconventional Searches for Exotic Particles at Future Lepton Colliders*, *EPJ Web Conf.* **315** (2024) 01034, [[arXiv:2412.14560](#)].
- [45] W. Altmannshofer and P. Munbodh, *Probing Lepton Flavor Violation at Linear Electron-Positron Colliders*, [arXiv:2505.11653](#).
- [46] “International Muon Collider Collaboration.” <https://muoncollider.web.cern.ch/>.
- [47] D. Schulte, J.-P. Delahaye, M. Diemoz, K. Long, B. Mansoulié, N. Patrone, L. Rivkin, A. M. Skrinsky, and A. Wulzer, *Muon Collider. A Path to the Future?*, *PoS EPS-HEP2019* (2020) 004.
- [48] J. P. Delahaye, M. Diemoz, K. Long, B. Mansoulié, N. Pastrone, L. Rivkin, D. Schulte, A. Skrinsky, and A. Wulzer, *Muon Colliders*, [arXiv:1901.06150](#).
- [49] **International Muon Collider** Collaboration, D. Schulte, *The Muon Collider*, *JACoW IPAC2022* (2022) 821–826.
- [50] **International Muon Collider** Collaboration, C. Accettura et al., *Interim report for the International Muon Collider Collaboration (IMCC)*, *CERN Yellow Rep. Monogr.* **2/2024** (2024) 176, [[arXiv:2407.12450](#)].
- [51] M. Begel et al., *United States Muon Collider Community White Paper for the European Strategy for Particle Physics Update*, [arXiv:2503.23695](#).
- [52] A. Costantini, F. De Lillo, F. Maltoni, L. Mantani, O. Mattelaer, R. Ruiz, and X. Zhao, *Vector boson fusion at multi-TeV muon colliders*, *JHEP* **09** (2020) 080, [[arXiv:2005.10289](#)].
- [53] T. Han, Y. Ma, and K. Xie, *High energy leptonic collisions and electroweak parton distribution functions*, *Phys. Rev. D* **103** (2021), no. 3 L031301, [[arXiv:2007.14300](#)].
- [54] T. Han, Y. Ma, and K. Xie, *Quark and gluon contents of a lepton at high energies*, *JHEP* **02** (2022) 154, [[arXiv:2103.09844](#)].
- [55] H. Al Ali et al., *The muon Smasher’s guide*, *Rept. Prog. Phys.* **85** (2022), no. 8 084201, [[arXiv:2103.14043](#)].
- [56] C. Accettura et al., *Towards a muon collider*, *Eur. Phys. J. C* **83** (2023), no. 9 864, [[arXiv:2303.08533](#)]. [Erratum: *Eur.Phys.J.C* 84, 36 (2024)].

- [57] **Muon Collider** Collaboration, J. de Blas et al., *The physics case of a 3 TeV muon collider stage*, [arXiv:2203.07261](#).
- [58] A. K. Barik, S. K. Rai, and A. Srivastava, *Discovering an invisible Z' at the muon collider*, *Phys. Lett. B* **866** (2025) 139533, [[arXiv:2408.14396](#)].
- [59] Y. Abe et al., *Status of the International Linear Collider*, [arXiv:2505.11292](#).
- [60] P. Chen, T. L. Barklow, and M. E. Peskin, *Hadron production in gamma gamma collisions as a background for e^+e^- linear colliders*, *Phys. Rev. D* **49** (1994) 3209–3227, [[hep-ph/9305247](#)].
- [61] T. Barklow et al., *Beam delivery and beamstrahlung considerations for ultra-high energy linear colliders*, *JINST* **18** (2023), no. 09 P09022, [[arXiv:2305.00573](#)].
- [62] **International Muon Collider** Collaboration, M. Casarsa et al., *Higgs physics prospects at a 3 TeV muon collider*, *PoS EPS-HEP2023* (2024) 408.
- [63] R. Franceschini, *Multiplexing new physics search at high-energy lepton colliders*, *Int. J. Mod. Phys. A* **37** (2022), no. 30 2246007.
- [64] N. Ghosh, S. K. Rai, and T. Samui, *Search for a leptiquark and vector-like lepton in a muon collider*, *Nucl. Phys. B* **1004** (2024) 116564, [[arXiv:2309.07583](#)].
- [65] T. Han, M. Low, T. A. Wu, and K. Xie, *Colorful Particle Production at High-Energy Muon Colliders*, [arXiv:2502.20443](#).
- [66] P. Asadi, A. Radick, and T.-T. Yu, *Interplay of freeze-in and freeze-out: Lepton-flavored dark matter and muon colliders*, *Phys. Rev. D* **110** (2024), no. 3 035022, [[arXiv:2312.03826](#)].
- [67] M. Chiesa, B. Mele, and F. Piccinini, *Multi Higgs production via photon fusion at future multi-TeV muon colliders*, *Eur. Phys. J. C* **84** (2024), no. 5 543, [[arXiv:2109.10109](#)].
- [68] K. Mękała, J. Reuter, and A. F. Żarnecki, *Optimal search reach for heavy neutral leptons at a muon collider*, *Phys. Lett. B* **841** (2023) 137945, [[arXiv:2301.02602](#)].
- [69] L. Zhao, H. Li, Z.-L. Han, F. Huang, and X. Yan, *Research of Extra Charged Gauge Boson W' in Alternative Left-Right Model at Future Muon Collider*, [arXiv:2412.05787](#).
- [70] J. Braathen, M. Gabelmann, T. Robens, and P. Stylianou, *Probing the Inert Doublet Model via vector-boson fusion at a muon collider*, *JHEP* **25** (2020) 055, [[arXiv:2411.13729](#)].
- [71] P. Bandyopadhyay and S. Parashar, *Probing a scalar singlet-triplet extension of the standard model via vector boson fusion at a muon collider*, *Phys. Rev. D* **110** (2024), no. 11 115032, [[arXiv:2410.06298](#)].
- [72] A. Belyaev, R. S. Chivukula, B. Fuks, E. H. Simmons, and X. Wang, *Vectorlike top quark production via an electroweak dipole moment at a muon collider*, *Phys. Rev. D* **108** (2023), no. 3 035016, [[arXiv:2306.11097](#)].
- [73] T. Li, C.-Y. Yao, and M. Yuan, *Searching for heavy neutral lepton and lepton number violation through VBS at high-energy muon colliders*, *JHEP* **09** (2023) 131, [[arXiv:2306.17368](#)].

- [74] F.-X. Yang, F.-L. Shao, Z.-L. Han, F. Huang, Y. Jin, and H. Li, *Lepton Number Violation Higgs Decay at Muon Collider*, [arXiv:2505.07331](#).
- [75] Q. Bi, J. Guo, J. Liu, Y. Luo, and X.-P. Wang, *Long-lived sterile neutrino searches at future muon colliders*, *Phys. Rev. D* **111** (2025), no. 7 075001, [[arXiv:2409.17243](#)].
- [76] F. Abu-Ajamieh, S. Modak, S. Mukherjee, and S. K. Vempati, *Pseudoscalar Higgs Production at Muon Colliders: The Role of One-Loop Effective Vertices*, [arXiv:2505.02092](#).
- [77] **International Muon Collider** Collaboration, C. Accettura et al., *The Muon Collider*, [arXiv:2504.21417](#).
- [78] N. Ghosh, S. K. Rai, and T. Samui, *Collider signatures of a scalar leptoquark and vectorlike lepton in light of muon anomaly*, *Phys. Rev. D* **107** (2023), no. 3 035028, [[arXiv:2206.11718](#)].
- [79] M. Mitra, S. Niyogi, and M. Spannowsky, *Type-II Seesaw Model and Multilepton Signatures at Hadron Colliders*, *Phys. Rev. D* **95** (2017), no. 3 035042, [[arXiv:1611.09594](#)].
- [80] D. K. Ghosh, N. Ghosh, I. Saha, and A. Shaw, *Revisiting the high-scale validity of the type II seesaw model with novel LHC signature*, *Phys. Rev. D* **97** (2018), no. 11 115022, [[arXiv:1711.06062](#)].
- [81] D. Kumar Ghosh, N. Ghosh, and B. Mukhopadhyaya, *Distinctive Collider Signals for a Two Higgs Triplet Model*, *Phys. Rev. D* **99** (2019), no. 1 015036, [[arXiv:1808.01775](#)].
- [82] R. Padhan, D. Das, M. Mitra, and A. Kumar Nayak, *Probing doubly and singly charged Higgs bosons at the pp collider HE-LHC*, *Phys. Rev. D* **101** (2020), no. 7 075050, [[arXiv:1909.10495](#)].
- [83] A. Jueid, T. A. Chowdhury, S. Nasri, and S. Saad, *Probing Zee-Babu states at muon colliders*, *Phys. Rev. D* **109** (2024), no. 7 075011, [[arXiv:2306.01255](#)].
- [84] T. Li, C.-Y. Yao, and M. Yuan, *Revealing the origin of neutrino masses through the Type II Seesaw mechanism at high-energy muon colliders*, *JHEP* **03** (2023) 137, [[arXiv:2301.07274](#)].
- [85] J.-C. Jia, Z.-L. Han, F. Huang, Y. Jin, and H. Li, *Production of single doubly charged Higgs bosons at muon colliders*, *Phys. Rev. D* **111** (2025), no. 1 015009, [[arXiv:2409.16582](#)].
- [86] S. P. Maharathy and M. Mitra, *Type-II see-saw at $\mu+\mu-$ collider*, *Phys. Lett. B* **844** (2023) 138105, [[arXiv:2304.08732](#)].
- [87] M. Aoki and D. Kaneko, *A hybrid seesaw model and hierarchical neutrino flavor structures based on A_4 symmetry*, *PTEP* **2021** (2021), no. 2 023B06, [[arXiv:2009.06025](#)].
- [88] A. Zee, *Quantum Numbers of Majorana Neutrino Masses*, *Nucl. Phys. B* **264** (1986) 99–110.
- [89] K. S. Babu, *Model of 'Calculable' Majorana Neutrino Masses*, *Phys. Lett. B* **203** (1988) 132–136.
- [90] P. S. Bhupal Dev and Y. Zhang, *Displaced vertex signatures of doubly charged scalars in the type-II seesaw and its left-right extensions*, *JHEP* **10** (2018) 199, [[arXiv:1808.00943](#)].
- [91] Y. Cheng, X.-G. He, Z.-L. Huang, and M.-W. Li, *Type-II seesaw triplet scalar effects on neutrino trident scattering*, *Phys. Lett. B* **831** (2022) 137218, [[arXiv:2204.05031](#)].

- [92] **MEG** Collaboration, A. M. Baldini et al., *Search for the lepton flavour violating decay $\mu^+ \rightarrow e^+ \gamma$ with the full dataset of the MEG experiment*, *Eur. Phys. J. C* **76** (2016), no. 8 434, [[arXiv:1605.05081](#)].
- [93] **SINDRUM** Collaboration, U. Bellgardt et al., *Search for the Decay $\mu^+ \rightarrow e^+ e^+ e^-$* , *Nucl. Phys. B* **299** (1988) 1–6.
- [94] **BaBar** Collaboration, B. Aubert et al., *Searches for Lepton Flavor Violation in the Decays $\tau_{+-} \rightarrow e_{+-} \gamma$ and $\tau_{+-} \rightarrow \mu_{+-} \gamma$* , *Phys. Rev. Lett.* **104** (2010) 021802, [[arXiv:0908.2381](#)].
- [95] **Belle** Collaboration, A. Abdesselam et al., *Search for lepton-flavor-violating tau-lepton decays to $\ell \gamma$ at Belle*, *JHEP* **10** (2021) 19, [[arXiv:2103.12994](#)].
- [96] K. Hayasaka et al., *Search for Lepton Flavor Violating Tau Decays into Three Leptons with 719 Million Produced $\tau^+ \tau^-$ Pairs*, *Phys. Lett. B* **687** (2010) 139–143, [[arXiv:1001.3221](#)].
- [97] L. Willmann et al., *New bounds from searching for muonium to anti-muonium conversion*, *Phys. Rev. Lett.* **82** (1999) 49–52, [[hep-ex/9807011](#)].
- [98] **DELPHI** Collaboration, J. Abdallah et al., *Measurement and interpretation of fermion-pair production at LEP energies above the Z resonance*, *Eur. Phys. J. C* **45** (2006) 589–632, [[hep-ex/0512012](#)].
- [99] G. C. Branco, P. M. Ferreira, L. Lavoura, M. N. Rebelo, M. Sher, and J. P. Silva, *Theory and phenomenology of two-Higgs-doublet models*, *Phys. Rept.* **516** (2012) 1–102, [[arXiv:1106.0034](#)].
- [100] **ATLAS** Collaboration, G. Aad et al., *Search for doubly charged Higgs boson production in multi-lepton final states using 139 fb^{-1} of proton–proton collisions at $\sqrt{s} = 13 \text{ TeV}$ with the ATLAS detector*, *Eur. Phys. J. C* **83** (2023), no. 7 605, [[arXiv:2211.07505](#)].
- [101] A. Alloul, N. D. Christensen, C. Degrande, C. Duhr, and B. Fuks, *FeynRules 2.0 - A complete toolbox for tree-level phenomenology*, *Comput. Phys. Commun.* **185** (2014) 2250–2300, [[arXiv:1310.1921](#)].
- [102] J. Alwall, M. Herquet, F. Maltoni, O. Mattelaer, and T. Stelzer, *MadGraph 5 : Going Beyond*, *JHEP* **06** (2011) 128, [[arXiv:1106.0522](#)].
- [103] T. Sjöstrand, S. Ask, J. R. Christiansen, R. Corke, N. Desai, P. Ilten, S. Mrenna, S. Prestel, C. O. Rasmussen, and P. Z. Skands, *An introduction to PYTHIA 8.2*, *Comput. Phys. Commun.* **191** (2015) 159–177, [[arXiv:1410.3012](#)].
- [104] **DELPHES 3** Collaboration, J. de Favereau, C. Delaere, P. Demin, A. Giammanco, V. Lemaître, A. Mertens, and M. Selvaggi, *DELPHES 3, A modular framework for fast simulation of a generic collider experiment*, *JHEP* **02** (2014) 057, [[arXiv:1307.6346](#)].
- [105] C. Collaboration, “Delphes card for muon collider.” https://indico.cern.ch/event/957299/contributions/4023467/attachments/2106044/3541874/delphes_card_mucol_mdi_.pdf, 2020.
- [106] G. Cowan, K. Cranmer, E. Gross, and O. Vitells, *Asymptotic formulae for likelihood-based tests of new physics*, *Eur. Phys. J. C* **71** (2011) 1554, [[arXiv:1007.1727](#)]. [Erratum: *Eur.Phys.J.C* **73**, 2501 (2013)].

- [107] B. Bhattacharjee, A. Kundu, S. K. Rai, and S. Raychaudhuri, *Universal Extra Dimensions, Radiative Returns and the Inverse Problem at a Linear e^+e^- Collider*, *Phys. Rev. D* **78** (2008) 115005, [[arXiv:0805.3619](#)].